CBP30, a selective CBP/p300 bromodomain inhibitor, suppresses human Th17 responses

Ariane Hammitzsch[a], Cynthia Tallant[b,c], Oleg Fedorov[b,c], Alison O'Mahony[d], Paul E. Brennan[b,c], Duncan A. Hay[b,1], Fernando O. Martinez[a], M. Hussein Al-Mossawi[a], Jelle de Wit[a], Matteo Vecellio[a], Christopher Wells[b,2], Paul Wordsworth[a], Susanne Müller[b,c], Stefan Knapp[b,c,e,3], and Paul Bowness[a,3]

[a]Botnar Research Institute, Nuffield Department of Orthopaedics, Rheumatology, and Musculoskeletal Science, University of Oxford, Oxford OX3 7LD, United Kingdom; [b]Structural Genomics Consortium, Nuffield Department of Clinical Medicine, University of Oxford, Oxford OX3 7DQ, United Kingdom; [c]Target Discovery Institute, Nuffield Department of Clinical Medicine, University of Oxford, Oxford OX3 7FZ, United Kingdom; [d]BioSeek Division of DiscoveRx Corporation, South San Francisco, CA 94080; and [e]Institute for Pharmaceutical Chemistry, Johann Wolfgang Goethe-University, 60438 Frankfurt am Main, Germany

Edited by Saadi Khochbin, Université Joseph Fourier, INSERM U823, Grenoble, France, and accepted by the Editorial Board July 13, 2015 (received for review January 29, 2015)

Th17 responses are critical to a variety of human autoimmune diseases, and therapeutic targeting with monoclonal antibodies against IL-17 and IL-23 has shown considerable promise. Here, we report data to support selective bromodomain blockade of the transcriptional coactivators CBP (CREB binding protein) and p300 as an alternative approach to inhibit human Th17 responses. We show that CBP30 has marked molecular specificity for the bromodomains of CBP and p300, compared with 43 other bromodomains. In unbiased cellular testing on a diverse panel of cultured primary human cells, CBP30 reduced immune cell production of IL-17A and other proinflammatory cytokines. CBP30 also inhibited IL-17A secretion by Th17 cells from healthy donors and patients with ankylosing spondylitis and psoriatic arthritis. Transcriptional profiling of human T cells after CBP30 treatment showed a much more restricted effect on gene expression than that observed with the pan-BET (bromo and extraterminal domain protein family) bromodomain inhibitor JQ1. This selective targeting of the CBP/p300 bromodomain by CBP30 will potentially lead to fewer side effects than with the broadly acting epigenetic inhibitors currently in clinical trials.

CBP/p300 | bromodomain | epigenetic inhibitors | Th17 | ankylosing spondylitis

Bromodomain recognition of acetylated lysines in histones plays a key role in the epigenetic control of gene expression (1). Therapeutic targeting of bromodomains has recently been recognized as an important potential therapeutic modality in human malignant and inflammatory diseases (2–4).

The transcriptional coactivators CBP [also known as cAMP responsive element binding protein (CREB) binding protein] and the closely related p300 possess such a bromodomain (5). Strategies targeting catalytic histone acetyl transferase (HAT) activity (6), the N-terminal domain (7), or the KIX (kinase-inducible domain interacting) domain (8) have had variable efficacy. By contrast, most bromodomain acetyl-lysine binding sites have good predicted druggability (9), confirmed experimentally by the recent development of potent and selective inhibitors targeting the bromo and extraterminal domain (BET) family (10–13). The promising effects of BET inhibitors observed in cancer cell lines have stimulated the rapid optimization of these tool molecules to yield clinical candidate drugs (2). A number of weak inhibitors, such as ischemin (K_D = 25 μM), have been reported to target the CBP/p300 bromodomain (14). The synthesis and binding modes of more potent CBP and BET/CBP inhibitors have been reported in the last year (15, 16). The most potent of these inhibitors, CBP30, has recently been shown to bind with low nanomolar affinity to the bromodomains of CBP/p300 (15). However, this initial study did not examine the broader specificity of CBP30 for other bromodomain targets or look at the ability of CBP30 to inhibit physiological cellular processes.

BET bromodomain inhibitors exhibit antiinflammatory activity by inhibiting expression of inflammatory genes (11). The pan-BET inhibitor JQ1 ameliorated collagen-induced arthritis and experimental autoimmune encephalomyelitis (17), both mouse models of human inflammatory disease with major Th17 components. Th17 cells, a subset of T helper cells producing IL-17A, IL-17F, IL-21, IL-22, and GM-CSF, have been identified as central effectors of several autoimmune diseases, including ankylosing spondylitis (AS), psoriasis and psoriatic arthritis (PSA), rheumatoid arthritis, Crohn's disease, and multiple sclerosis (18–20). AS is a common chronic inflammatory disease affecting ~0.2–0.5% of adults in the United States. AS is characterized by inflammation of the sacroiliac and spinal joints leading to bony fusion (ankylosis), pain, and disability. Treatment options have until recently been limited

Significance

Epigenetic inhibitors have shown considerable promise for the treatment of malignant and inflammatory diseases. We present here the detailed characterization of a potent and highly selective inhibitor of the bromodomains of CBP (CREB binding protein)/p300. Functional preclinical data studying cells derived from patients with ankylosing spondylitis and psoriatic arthritis (two human Th17-driven diseases) show that selective inhibition of the CBP/p300 bromodomain with CBP30 strongly reduces secretion of IL-17A, without having the broader and potentially deleterious effects on cytokine production and gene transcription of the pan-BET (bromo and extraterminal domain protein family) inhibitor JQ1. CBP/p300 play a significant role in IL-17A production, and CBP/p300 inhibition is a promising therapeutic strategy in human type-17–mediated diseases such as ankylosing spondylitis and psoriatic arthritis.

Author contributions: A.H., F.O.M., P.W., S.K., and P.B. designed research; A.H., C.T., O.F., A.O'M., P.E.B., D.A.H., M.H.A.-M., J.d.W., M.V., C.W., and S.M. performed research; A.H., F.O.M., S.K., and P.B. analyzed data; and A.H., S.K., and P.B. wrote the paper.

Conflict of interest statement: P.B. declares research support from Merck Research Laboratories.

This article is a PNAS Direct Submission. S.K. is a guest editor invited by the Editorial Board.

Data deposition: The microarray data reported in this paper have been deposited in the Gene Expression Omnibus (GEO) database, www.ncbi.nlm.nih.gov/geo (accession no. GSE71231). The models and structure factors have been deposited in the Protein Data Bank, www.pdb.org {PDB ID codes 5BT3 [EP300], 5BT4 [BRD4(1)], and 5BT5 [BRD2(2)]}.

[1]Present address: Evotec (UK) Ltd., Milton Park, Abingdon OX14 4RZ, United Kingdom.

[2]Present address: Nanotether Discovery Sciences Ltd., Cardiff University, Cardiff CF10 3AX, United Kingdom.

[3]To whom correspondence may be addressed. Email: paul.bowness@ndorms.ox.ac.uk or knapp@pharmchem.uni-frankfurt.de.

This article contains supporting information online at www.pnas.org/lookup/suppl/doi:10.1073/pnas.1501956112/-/DCSupplemental.

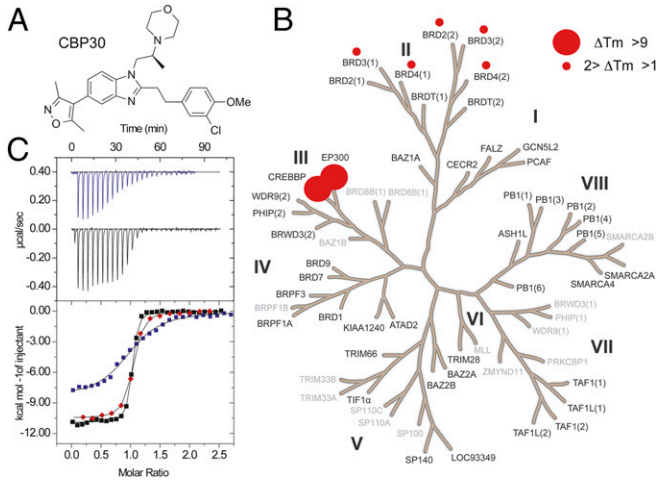

Fig. 1. CBP30 is a selective and potent inhibitor of CBP/p300. (*A*) Chemical structure of CBP30. (*B*) Temperature shift data covering 45 human bromodomains. Screened targets are highlighted in black and targets that have not been screened in gray. Temperature shifts are represented by spheres. The gene name *CREBBP* corresponds to CBP protein, and *EP300* to the protein p300. (*C*) Isothermal titration calorimetry data measuring the binding of CBP30 to BRD4 (blue), CBP (red), and p300 (black). (Upper) Raw injection heats for BRD4(1) and p300. (*Lower*) Normalized binding heats [BRD4(1), CBP, p300]. Nonlinear least squares fits to a single binding site model are shown as solid lines.

to nonsteroidal antiinflammatory agents and anti-TNF biologic agents (21). An anti–IL-17A antibody, secukinumab, proved efficacious in AS, further supporting the importance of Th17 cells in AS (22). This finding has intensified the search for new drug targets modulating cytokine production of Th17 cells. Cytokine-driven induction of the transcriptional Th17 profile is strongly mediated by epigenetic mechanisms (23), one facilitator being the transcriptional coactivator p300. Recent studies demonstrated that p300 binds to the *Il 17a* promoter in murine Th17 cells and facilitates chromatin accessibility (24).

Here, we show the potent and selective nature of inhibition of the CBP/p300 bromodomains by CBP30. We demonstrate that CBP30 inhibits IL-17A production in primary human cells and Th17 responses from patients with AS and PSA. The effect of this inhibitor is far more selective than that observed for the pan-BET bromodomain inhibitor JQ1. Our data identify a previously unidentified strategy targeting the CBP/p300 bromodomain in human inflammatory diseases with major Th17 contribution such as AS.

Results

CBP30 Preferentially Binds to the CBP/p300 Bromodomain. Synthetic variation on the 5-isoxazolyl-benzimidazole series of bromodomain inhibitors led to the development of CBP30 (Fig. 1*A*). Initial screening against 10 bromodomains suggested selectivity for CBP/p300 bromodomains (15). Here, we evaluated the selectivity of this inhibitor using temperature shift assays against a total of 45 bromodomains (Fig. 1*B* and Table S1), revealing only BET family bromodomains as additional targets. Notably, CBP30 did not result in significant ΔT_m shifts for the testis-specific isoform BRDT (bromodomain testis-specific protein) whereas the rest of the BET family [first and second bromodomains of (bromodomain-containing protein) BRD2, BRD3, and BRD4] showed ΔT_m shifts between 0.9 and 2.0 °C, suggesting low μM dissociation constants. We used isothermal titration calorimetry (ITC) to determine the dissociation constants (K_Ds) in solution for the bromodomains of CBP/p300 and other BET family members. ITC data revealed K_Ds of 26 nM and 32 nM for CBP and p300, respectively (Fig. 1*C*), in good agreement with affinity data already reported (15). Within the BET family, the first bromodomain of BRD4 [BRD4(1)] bound with highest affinity (K_D of 885 nM), thus with 34-fold reduced selectivity compared with CBP (Table S2).

Molecular Details of the Interaction of CBP30 with p300, BRD4, and BRD2. To understand the structural mechanisms for the selectivity of CBP30 for specific BET family members, we determined the cocrystal structure of CBP30 with the p300, BRD4(1), and BRD2(2) bromodomains. Crystals of the CBP30/p300 complex diffracted to 1.05 Å resolution (Table S3). As observed in the CBP bromodomain cocrystal structure (PDB ID code 4nr7), the CBP isoxazole oxygen acted as an acetyl-lysine mimetic moiety forming hydrogen bonds to the conserved asparagine (N1132) and a water-mediated interaction with the hydroxyl group of Y1089 of p300 (Fig. 2*A*). However, and in contrast to the CBP complex, we did not observe an induced fit binding mode of R1137, which has been reported to flip into the acetyl-lysine binding side forming a cation-π interaction. The reason for this difference in ligand coordination is due to the presence of a neighboring tyrosine residue (Y1141) that engages into a hydrogen bond interaction with R1137. In the CBP bromodomain, this position is occupied by a phenylalanine, allowing the arginine to stack with the aromatic decoration of the inhibitor. This induced fit has also been observed for other CBP bromodomain inhibitors (16). In the p300/CBP30 complex, the benzimidazole ring system was shifted, resulting in rotation of the morpholine moiety and the 3-chloro-4-methoxyphenol ring system (Fig. 2*B*). Additional comparison of CBP30 binding to p300 with BRD4(1) and BRD2(2) is shown in Fig. S1.

Kinetics of CBP30 Binding to CBP/p300. Bio-layer interference (BLI) showed similar rapid dissociation rates of CBP30 with p300 and CBP (Fig. 3 *A* and *B*). K_D values calculated from the steady-state dose–response curves were 38 ± 4.7 nM and 47 ± 2.1 nM for CBP and p300, respectively, in good agreement with ITC data. Analysis of ligand-binding kinetics showed both fast and comparable dissociation on and off rates (CBP, k_{on}, 3.21 ± 0.28 × 10^5 $M^{-1}{\cdot}s^{-1}$ and k_{dis}, 1.42 ± 0.04 × 10^{-2} s^{-1}; and p300, k_{on} 1.43 ± 0.19 × 10^5 $M^{-1}{\cdot}s^{-1}$ and k_{dis}, 9.05 ± 0.22 × 10^{-3} s^{-1}). Thus, the induced fit binding mode observed in CBP bromodomain complexes does not contribute to slow binding kinetics of CBP30.

We used the fluorescent recovery after photobleaching (FRAP) assay to measure the displacement of the CBP bromodomain from chromatin in the presence of CBP30 (25). A GFP-labeled construct containing three CBP bromodomains flanked by a nuclear localization signal (NLS) showed significantly reduced recovery half-life in the presence of CBP30 (Fig. 3 *C* and *D*), comparable with the inactivating bromodomain mutant N1132F. By contrast, BRD4 recovery rates were only modestly affected, compared with

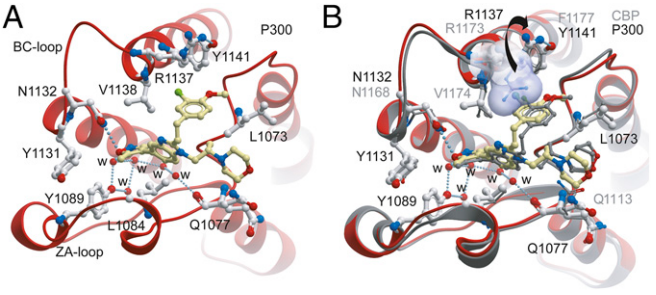

Fig. 2. Comparison of CBP30 binding to the p300 and CBP bromodomains. (*A*) Binding of CBP30 to p300. The inhibitor and most important interacting side chains are shown in ball and stick representation. Conserved water molecules are highlighted as red spheres and are labeled with "w." Hydrogen bonds are shown as dotted lines. (*B*) Comparison of the CBP30 binding modes in the CBP and p300 bromodomain complex (15). The side chain of R1173 in CBP is shown in surface representation and is indicated by an arrow.

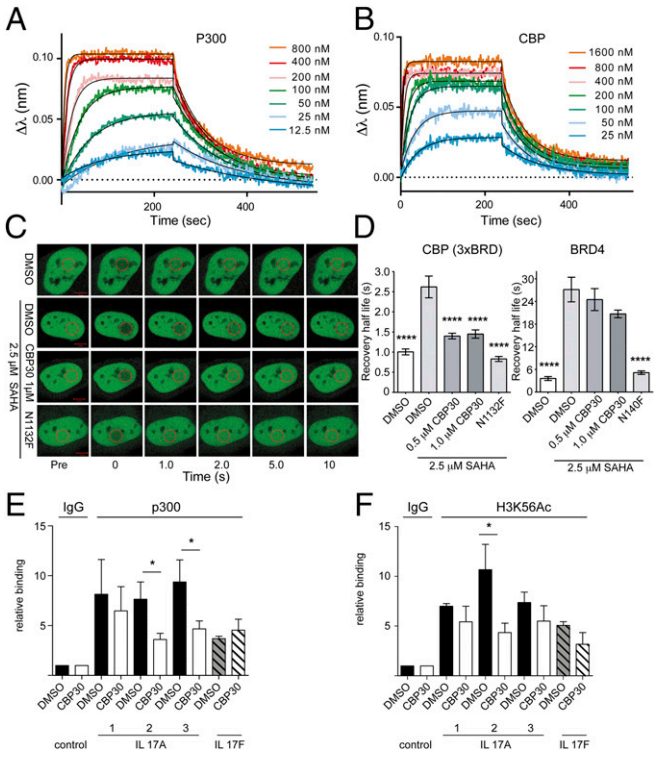

Fig. 3. CBP30 binding kinetics and nuclear target engagement. Sensograms monitoring the kinetics of CBP30 association and dissociation with p300 (*A*) and with CBP (*B*) using BLI (bio-layer interferometry). (*C*) FRAP using 3× CBP BRD. Shown are nuclei of transfected cells. The bleached area is indicated by a red circle before (Pre), at bleaching (time = 0), and post-bleaching as indicated. (*D*) Averaged recovery half-life ($n = 10$) of DMSO, DMSO/SAHA (2.5 μM), and CBP30 (1 μM)/SAHA (2.5 μM) treated 3× CBP BRD or BRD4-transfected cells. Raw data traces of the fluorescent recovery are shown in Fig. S2. The pan-HDAC inhibitor SAHA was used to increase global acetylation (25). One-way ANOVA, $^{****}P < 0.0001$. CBP30 reduces p300 (*E*) and H3K56Ac (*F*) binding to the *IL 17A* gene locus. ChIP-q-PCR assessed in three different regions (regions 1–3) of the *IL 17A* and in one region of the *IL 17F* locus in Th17 cells treated with 2 μM CBP30 or DMSO for 24 h. Relative enrichment is expressed as mean ± SEM of four (*E*) and three (*F*) independent experiments (Student's *t* test); $^{*}P < 0.05$.

the inactivating mutant N140F. CBP30 also inhibited binding of p300 and of acetylated histone H3K56 (a known CBP/p300 mark) to the *IL 17A* gene locus in chromatin immunoprecipitation experiments (Fig. 3 *E* and *F*).

Antiinflammatory Activity of CBP30 on Primary Human Cells. The biological activity of CBP30 was explored using a panel of 12 stimulated primary human cell types (BioMAP) (26, 27). This analysis revealed broad antiinflammatory activity but no pronounced cytotoxicity at concentrations up to 10 μM. Potential immunomodulatory effects observed included down-regulation of the cytokines IL-17, TNFα, IL-8, IL-2, IL-6, IL-1α, and IL-10, vascular cell adhesion protein 1 (VCAM-1), and cytokine monocyte chemotactic protein 1 (MCP1) (Fig. 4*A* and Fig. S3). In addition, inhibition of matrix metalloproteinases MMP-1 and MMP-9 and of tissue plasminogen activator (tPA) suggested potential modulation of matrix/tissue remodeling by CBP30. The BioMAP profile showed overlap with BET inhibitor profiles at high inhibitor concentrations (3.3 and 10 μM). This overlap may be due to weak BET activity of CBP30 or to coregulation of similar signaling molecules by CBP/p300 and BET (Fig. 4*B* and Figs. S3 and S4). Nevertheless, a distinct phenotype was detected at lower concentrations, suggesting that CBP30 does not affect BET function in cells at these concentrations (Fig. S4).

CBP30 Inhibits Th17 Cytokine Production from Patient and Control T Cells. We measured cytokine secretion (ELISA) by purified $CD4^+$ T cells from AS and PSA patients and healthy controls (HCs) cultured for 3 d under Th17-promoting conditions. An initial dose–response experiment showed that 2 μM CBP30 inhibited IL-17A production by AS CD4 T cells by 77% (Fig. 5*A*). This concentration did not affect cell viability or proliferation (Fig. S5). JQ1 inhibited IL-17A secretion at lower concentrations but also showed evidence of toxicity at concentrations above 100 nM (Fig. S5). In subsequent experiments, JQ1 was used at 150 nM [the concentration used by Mele et al. (17)] and CBP30 at 2 μM. CBP30 on average reduced the secretion of IL-17A by 66.3% in cells from patients with AS and PSA and from HCs (Fig. 5*B*).

We next studied the additional Th17-associated cytokines IL-17F, GM-CSF, and IL-22. CBP30 (2 μM) caused only 14.6% inhibition of IL-17F production whereas 150 nM JQ1 reduced IL-17F by up to 85% (Fig. 5*A*). These results were confirmed for AS and PSA patients and for HCs (Fig. 5*B*). Secretion of the Th17-associated proinflammatory cytokine GM-CSF was significantly lowered by both CBP30 and JQ1, in both AS and PSA patients (Fig. 5*C*). IL-22 was not significantly inhibited (Fig. 5*D*). To determine the specificity for Th17 cells, we analyzed supernatants by ELISA for IFNγ, a key cytokine produced by Th1 cells. CBP30 had less effect than JQ1

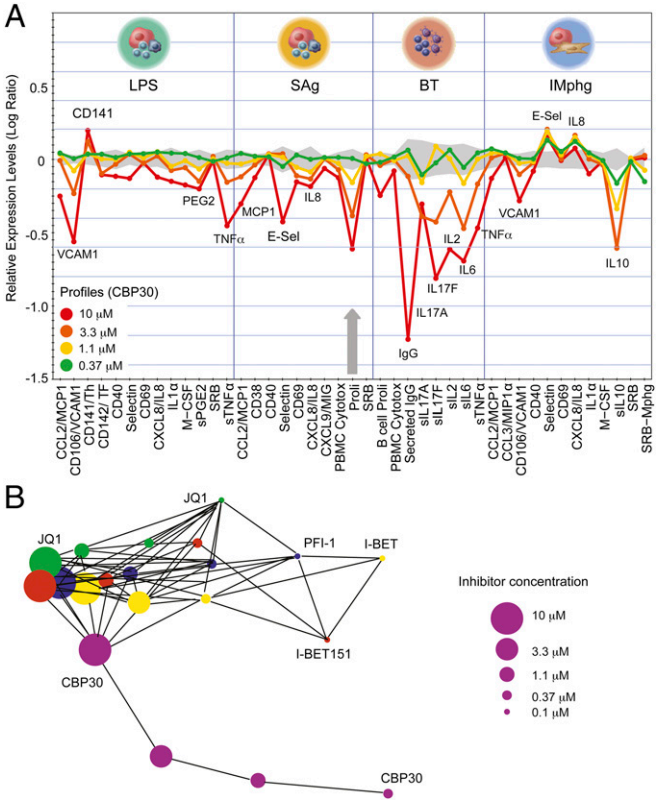

Fig. 4. BioMAP profile of CBP30 on primary hematopoietic cells. (*A*) CBP30 profile at 0.37–10 μM. Monitored marker proteins are shown on the *x* axis, and relevant proteins have been highlighted. Historic variations of DMSO-treated cells are indicated by the gray shaded area, and antiproliferative effects by gray arrows. A full BioMAP including other cell types is shown in Fig. S3. Studied cell systems were as follows: peripheral blood mononuclear cells plus venular endothelial cells stimulated with LPS or SEB (SAg); B cells plus peripheral blood mononuclear cells (BT); macrophages plus venular endothelial cells (IMphg). (*B*) Gleason correlation (>0.85) comparing the phenotypic response (Biomap profiles across all primary tissues) of CBP30 (purple circles) with the pan-BET inhibitors (JQ1 in green, I-BET in yellow, PFI-1 in blue, and I-BET151 in red). Concentrations from 0.1 to 10 μM are indicated by the size of the circles.

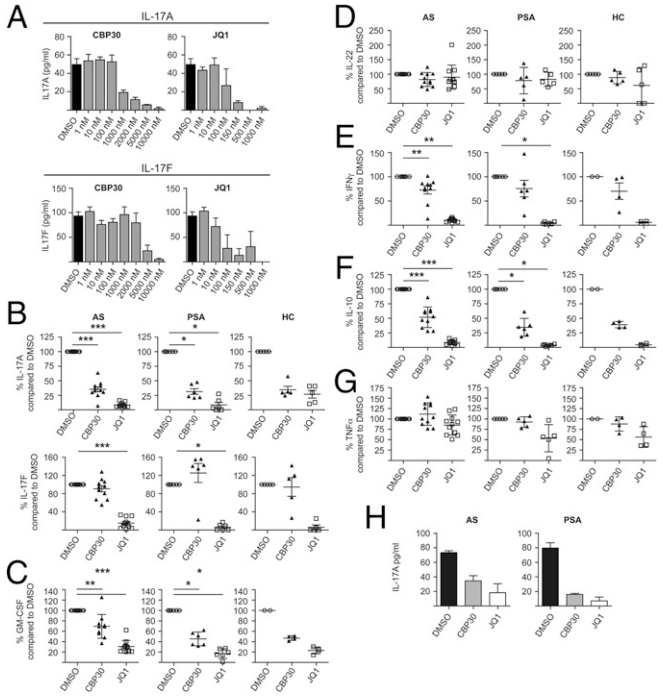

Fig. 5. CBP30 inhibits Th17 cytokine production by patient and control CD4 T cells. (*A*) IL-17A and F production from CD4$^+$ T cells from one AS patient cultured under Th17-promoting conditions in the presence of DMSO, CBP30, or JQ1 at concentrations from 1 nM to 10 μM. ELISA of supernatant on day three. Mean ± SD of triplicates of one representative experiment (n = 4). (*B*) IL-17A and F production from total CD4$^+$ T cells from 11 AS patients, 6 PSA patients, and 5 HCs cultured as in *A* in the presence of 2 μM CBP30 or 150 nM JQ1. Day 3 ELISA. Mean ± SEM, each triplicates. (*C*) GM-CSF and (*D*) IL-22 (LUMINEX) levels from AS patients, PSA patients, and HCs after inhibition with 2 μM CBP30 or 150 nM JQ1. Mean ± SD, n = 4–11. (*E*) IFNγ ELISA, mean ± SEM, (*F*) IL-10, and (*G*) TNFα (LUMINEX), mean ± SD, n = 4–11. (*H*) ELISA for IL-17A in the supernatant of CD4$^+$ T cells from synovial fluid of patients with AS and PSA cultured as in *A* in the presence of 2 μM CBP30 and 150 nM JQ1. Data represent one of two independent experiments in triplicate, mean ± SEM. Patient demographics shown in Table S4. Wilcoxon matched-pairs signed rank test (*P < 0.05; **P < 0.01; ***P < 0.001; no asterisk, P > 0.05).

on IFNγ or IL-10 secretion (Fig. 5 *E* and *F*) and did not affect TNF α secretion (Fig. 5*G*). Both CBP30 and JQ1 inhibited IL-17A production by synovial fluid CD4$^+$ T cells obtained from inflamed joints of two AS and two PSA patients (Fig. 5*H*). These data show that CBP30 has a more specific inhibitory effect on Th17 cytokines than JQ1.

CBP30 Has Narrower Effects on CD4 T-Cell Gene Expression than JQ1. Because the observed effects of CBP30 and JQ1 on Th17-type responses lie most likely in altered transcriptional activity, we compared gene expression of unstimulated HC CD4$^+$ T cells with cells cultured for 4 d in the presence of CBP30, JQ1, or DMSO. Although Th17-promoting conditions were used, because the starting percentages of Th17 cells were extremely low, Th17 cells made up <5% of the final lymphocyte population. During this period of stimulation, 2,087 transcripts representing 1,634 genes were significantly regulated (Fig. 6*A*). Fewer genes were uniquely up- or down-regulated by CBP30 than by JQ1 (42 and 18 by CBP30, respectively, vs. 125 and 120 by JQ1). Genes that were specifically up-regulated by JQ1 included genes of the histone clusters 1, 2, and 3, as well as *MIR155HG* and *CCL17* (Fig. 6 *B–D*). By contrast, CBP30 had a far more limited effect on gene expression (Fig. 6 *B–D*).

We further compared Th17-associated transcript expression by q-PCR in CD4$^+$ T cells from three additional HCs and three AS patient samples cultured under Th17-favorable conditions. Both CBP30 and JQ1 significantly reduced *IL 17A* and *IL 21* transcript levels in HC and AS patients (Fig. 6*E*). By contrast *IL 17F* transcripts were only significantly inhibited by JQ1 in AS patient samples. *IL 22* transcript levels were significantly reduced by CBP30 in HC and AS patients and by JQ1 in AS patients. *CSF2* levels were not significantly altered by either inhibitor. The expression of the Th17 lineage-stabilizing IL-23 Receptor (*IL 23R*) was significantly down-regulated by both inhibitors in HC CD4$^+$ T cells. Transcription of the Th17 master regulator *RORC* was reduced by JQ1 in HC and AS patients, and by CBP30 in AS CD4$^+$ T cells. Expression of *TBX21*, a Th1-associated transcription factor, was reduced significantly only in HC CD4$^+$ T cells, and the Th1 cytokine *IFNG* was inhibited only by JQ1. *IL 10* transcript expression was significantly reduced only in HC CD4$^+$ T cells. Thus, CBP30 has relative selectivity for Th17-associated genes whereas JQ1 has widespread effects on many gene families.

Discussion

In this work, we show that CBP30 is a highly selective inhibitor of the bromodomains of the transcriptional coactivators CBP and

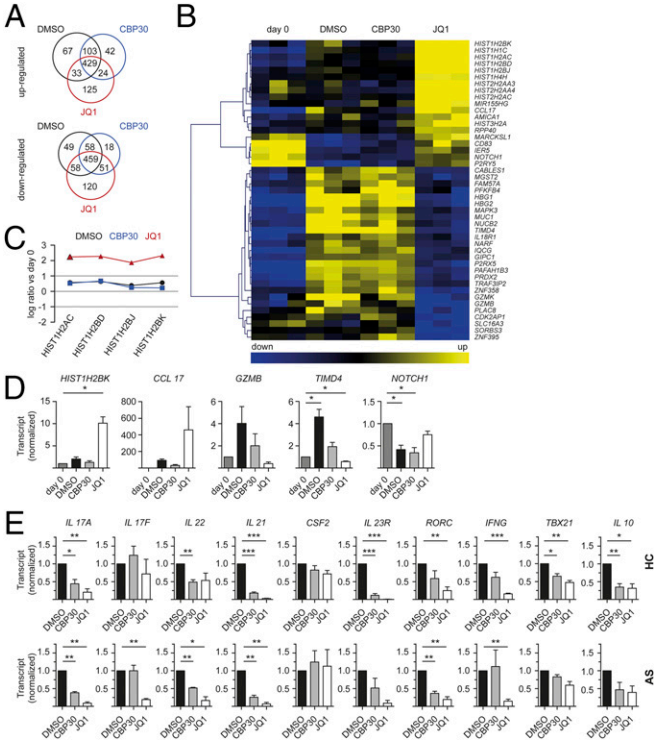

Fig. 6. CBP30 has more specific effects on CD4 T-cell gene expression than JQ1. (*A–D*) Total CD4$^+$ T cells from three healthy controls were cultured under Th17-promoting conditions in the presence of DMSO, 2 μM CBP30, or 150 nM JQ1 for 4 d before total RNA isolation. (*A*) Venn diagram showing number of genes significantly up- or down-regulated greater than twofold (ANOVA < 0.05 analyzed for whole genome expression with Illumina beadchip array HT12v4.1). Pathway analysis shown in Dataset S1. (*B*) Hierarchical clustering heat map of selected genes showing differential regulation by CBP30 and JQ1 [genes up- or down-regulated by >1 log(2) ratio and difference >0.75 log(2) ratio between DMSO, CBP30, and JQ1]. Data from three donors are shown for each experiment. (*C*) Line diagram displaying up-regulation of the histone cluster genes by JQ1 but not by CBP30. (*D*) q-PCR on selected genes from the microarray that are differentially regulated between CBP30 and JQ1; mean ± SEM, n = 2–3, triplicates. (*E*) Total CD4$^+$ T cells from four HC and three AS patients were treated as in *A*, and q-PCR on selected genes was performed; mean ± SEM, n = 3–4, triplicates. Paired t test (*P < 0.05, **P < 0.01, ***P < 0.001).

p300. The ability of CBP30 to inhibit IL-17A secretion was identified using an unbiased screen of primary human cells (BioMAP). We further present preclinical efficacy in inhibiting Th17 immune responses from blood and joints of patients with two Th17-driven inflammatory diseases, ankylosing spondylitis and psoriatic arthritis. The development of epigenetic inhibitors is showing real promise in treating human disease. However, drug specificity is a key issue, with the need to avoid both predictable and unexpected off-target effects. We and others have previously described bromodomain inhibitors with broad specificity. For example, JQ1 has shown efficacy in treating both murine Th17-mediated disease and cancers in mouse models and in vitro studies (10, 17, 28). Nineteen clinical trials with BET inhibitors in oncology are underway. Nevertheless, JQ1 has very broad activity (for example, inhibiting testicular BRDT to cause testicular atrophy and reversible infertility) (29) and would not be an acceptable therapy for noncancerous diseases. Our data show that CBP30 has a far narrower specificity, both at the molecular and cellular level. We performed a detailed screen of 45 human bromodomains, greatly extending the work of Hay et al. (15), showing greater than 30-fold selectivity of CBP30 for CBP and p300 compared with other bromodomains. Of note, no binding to BRDT was detectable, and CBP30 showed only weak activity for the second bromodomains of BET proteins, a feature that may additionally contribute to its cytokine inhibitory specificity.

We show here the ability of CBP30 to profoundly inhibit secretion of the proinflammatory cytokine IL-17A by human T helper cells from healthy individuals and patients with AS and PSA. AS and PSA are common human inflammatory arthritides, both termed "seronegative," with a combined prevalence of approximately 1% (30, 31). Both have a major IL-17–driven component, evidenced by multiple genetic, immunological, and therapeutic studies (20, 22, 32, 33). Indeed, and unlike rheumatoid arthritis, clinical studies targeting the IL-17/-23 axis with monoclonal antibodies in both AS and PSA have yielded very promising results, comparable with those seen with anti-TNF agents (22, 34). All patients studied by us had established disease, and a significant number had active disease. CBP30 also inhibited IL-17A production by Th17 cells from actively inflamed joints, showing efficacy at the site of inflammation. Overall, our data convincingly show that CBP30 effectively inhibits IL-17A production by Th17 cells from patients with AS and PSA and from HCs.

Th17 cells are heterogeneous and capable of producing multiple additional inflammatory cytokines, including GM-CSF, IL-17F, IL-21, and IL-22. We show here that CBP30 also inhibits GM-CSF cytokine secretion. Th17 cells secreting additional cytokines have been described as being particularly pathogenic, with GM-CSF in particular implicated in rheumatoid arthritis (35). The observed discrepancy between inhibitory effects of CBP30 on GM-CSF secretion and *CSF2* transcription might be explained by minor differences in the experimental time course. Transcriptional analysis on a limited number of AS patients and HCs confirmed the inhibitory effects on *IL 17A* and also showed down-regulation of *IL 21, IL 22*, the transcription factor *RORC* (in AS patients), and the signature cytokine receptor *IL 23R* (in HCs). CBP30 (unlike JQ1) did not inhibit transcription or secretion of the closely related cytokine IL-17F. This observation suggests hitherto unappreciated differences in the transcriptional control of *IL 17A* and *IL 17F*. We observed no effect of CBP30 on production of TNFα (a cytokine important for protection against tuberculosis) and smaller effects of JQ1 on IL-10 and IFNγ secretion. Thus, future therapeutic use of CBP/p300 inhibitors could result in more specific inhibition of IL-17A and other Th17-type cytokines by Th cells.

Transcriptional profiling of human CD4 T cells showed that CBP30 has more limited effects and far greater specificity than JQ1. Global expression arrays illustrated that JQ1 has effects on approximately fourfold more genes than CBP30. Although the global microarray showed only a limited Th17 signature (e.g., *IL18R1*, *MIR155HG*, and *NOTCH1*), we were nevertheless easily able to confirm the effects of CBP30 (and JQ1) on Th17-specific gene transcription on Th cells from AS patients and HCs by q-PCR. Of note, even after culture, Th17 cells made up only 2.9–8.3% of the total Th cell population (from healthy donors), explaining the lack of an obvious Th17-specific signal. Th17 cells represent <1% of healthy peripheral blood T lymphocytes (36), rising to ∼1–2% in AS, PSA, and psoriasis patients (19, 20, 36).

Transcriptional control of Th17 responses is a multistep process, involving numerous transcription factors (37). CBP/p300 is thought to be involved at an early stage, consistent with our data showing key sensitivity of human *IL 17A* transcription to CBP/p300 inhibition (38, 39). In murine Th17 cells, conserved noncoding sequence 2 (CNS2) is important to drive *Il 17* gene transcription in coordination with RORγt and is bound by p300 (24). However, expression of *Il 17f* is only partially dependent on CNS2, a possible explanation for the CBP30 specificity.

We present here, to our knowledge, the first detailed characterization of CBP30, a potent and highly selective CBP/p300 bromodomain inhibitor. Functional preclinical data show effective inhibition of IL17A secretion, without the broader and potentially deleterious effects of the pan-BET inhibitor JQ1. CBP30 merits further investigation as a lead therapeutic compound for AS, PSA, and other human type-17–mediated autoimmune diseases, including psoriasis, inflammatory bowel disease, and multiple sclerosis (40–42).

Materials and Methods

Inhibitors. SGC-CBP30 (hereafter called CBP30) and (+)-JQ1 (hereafter called JQ1) were provided by the Structural Genomics Consortium (SGC), Oxford.

ITC and Thermal Shift Assay. Experiments were carried out on a VP-ITC microcalorimeter (MicroCal) at 15 °C in 50 mM Hepes, pH 7.5, 150 mM NaCl, using an initial injection of 2 μL, followed by 34 identical injections of 8 μL. The dilution heats, measured separately, were subtracted from the titration data. Thermodynamic parameters were calculated using $\Delta G = \Delta H - T\Delta S = -RT\ln K_B$, where ΔG, ΔH, and ΔS are the changes in free energy, enthalpy, and entropy of binding respectively. In all cases, a single binding site model was used. Thermal melting experiments were carried out using an Mx3005p Real Time PCR machine (Stratagene) as described (43).

BLI. cDNA encoding human bromodomains was cloned, expressed, and purified as previously described (10). Kinetic ligand-binding measurements were done using an OctetRed384 instrument (ForteBio). Biotinylated protein (0.05 mg/mL) was immobilized on Super Streptavidin Biosensors. Association and dissociation measurements were done in 25 mM Hepes, pH 7.4, 100 mM NaCl, 0.01% Tween at 25 °C, with association and dissociation times of 240 s. Compounds were prepared as 1:2.5 dilutions starting from 12 μM. Binding to the reference sensors (no protein attached) was subtracted before calculations. Binding constants were calculated using the ForteBio Analysis software provided by the manufacturer.

Crystallization, Data Collection, and Structure Solution. EP300 construct (Uniprot identifier as EP300_HUMAN Q09472-1 fragment 1048–1161), BRD4 construct (Uniprot identifier as BRD4_HUMAN O60885-1 fragment 44–168), and BRD2 construct (Uniprot identifier as BRD2_HUMAN P25440-1 fragment 344–455) were used for crystallographic studies as described in *SI Materials and Methods*. Data collection and refinement statistics are compiled in Table S3. The models and structure factors have PDB ID codes 5BT3 (EP300), 5BT4 [BRD4(1)], and 5BT5 [BRD2(2)].

FRAP. FRAP studies were performed as described in *SI Materials and Methods* and (25).

ChIP. ChIP-q-PCR was performed as described in *SI Materials and Methods*.

BioMAP Analysis of Primary Human Cells. BioMAP assays were performed as previously described (26, 27). Data for CBP30 were compared with pan-BET inhibitors (JQ1, I-BET, PFI-1, and I-BET151) (10–13).

Patient Samples. Heparinized venous blood (30 mL) was obtained from 14 patients with AS (modified New York criteria), 6 patients with PSA [Classification of Psoriatic

Arthritis (CASPAR) criteria], and 8 HCs. Table S4 shows patient demographics and medication. Ethical permission (COREC 06/Q1606/139 and Oxfordshire Research Ethics Committee B 07/Q1605/35) and informed consent were obtained. Leukocyte cones were acquired from National Health Service Blood and Transplant.

Cell Purification and Cell Culture, ELISA, and LUMINEX Analysis. CD4 T cells (5×10^4, negatively selected: 89.1% purity) were cultured in 96-well plates in conditions that promoted Th17 numbers and preserved Th1, Th2, and Treg numbers as described in *SI Materials and Methods*. Supernatants were analyzed with an IL-17A, IL-17F, and IFNγ ELISA kit (ebioscience) and subjected to LUMINEX analysis with a custom-made premixed Multiplex Screening Assay for IL-10, IL-22, TNFα, and GM-CSF (R&D Systems).

Transcriptional Profiling. CD4 T cells (1×10^6) were cultured in 48-well plates, as described above, for 4 d. Microarray analysis of RNA used Illumina beadchip array HT12v4.1. Details are in *SI Materials and Methods*. For quantitative PCR (q-PCR), RNA was reverse transcribed with the High Capacity cDNA Reverse Transcription Kit (Applied Biosystems). TaqMan probes for transcripts encoding *IL 17A, IL 17F, IL 21, IL 22, CSF2, IL 10, IFNG, IL 23R, RORC, TBX21, HIST1H2BK, CCL17, GZMB, TIMD4*, and *NOTCH1* (see *SI Materials and Methods* for details) were used for q-PCR on a ViiA 7 Real-Time PCR System (Life Technologies).

Statistical Analysis. Statistical analysis was performed using GraphPad Prism software version 5. *P* values less than 0.05 were considered statistically significant.

ACKNOWLEDGMENTS. A.H. was funded by Deutsche Forschungsgemeinschaft Grant HA 7021/1-1. This work was funded by the Oxford National Institute for Health Research Biomedical Research Centre/Unit and by the Structural Genomics Consortium, a registered charity (number 1097737) that receives funds from AbbVie, Bayer Pharma AG, Boehringer Ingelheim, the Canada Foundation for Innovation, Genome Canada, GlaxoSmithKline, Janssen, Lilly Canada, the Novartis Research Foundation, the Ontario Ministry of Economic Development and Innovation, Pfizer, Takeda, and Wellcome Trust Grant 092809/Z/10/Z. P.B. is in part funded by the Innovative Medicines Initiative (IMI)-funded project Unrestricted Leveraging of Targets for Research Advancement and Drug Discovery (ULTRA-DD).

1. Delvecchio M, Gaucher J, Aguilar-Gurrieri C, Ortega E, Panne D (2013) Structure of the p300 catalytic core and implications for chromatin targeting and HAT regulation. *Nat Struct Mol Biol* 20(9):1040–1046.
2. Filippakopoulos P, Knapp S (2014) Targeting bromodomains: Epigenetic readers of lysine acetylation. *Nat Rev Drug Discov* 13(5):337–356.
3. Muller S, Filippakopoulos P, Knapp S (2011) Bromodomains as therapeutic targets. *Expert Rev Mol Med* 13:e29.
4. Belkina AC, Nikolajczyk BS, Denis GV (2013) BET protein function is required for inflammation: Brd2 genetic disruption and BET inhibitor JQ1 impair mouse macrophage inflammatory responses. *J Immunol* 190(7):3670–3678.
5. Vo N, Goodman RH (2001) CREB-binding protein and p300 in transcriptional regulation. *J Biol Chem* 276(17):13505–13508.
6. Arif M, et al. (2009) Mechanism of p300 specific histone acetyltransferase inhibition by small molecules. *J Med Chem* 52(2):267–277.
7. Emami KH, et al. (2004) A small molecule inhibitor of beta-catenin/CREB-binding protein transcription [corrected]. *Proc Natl Acad Sci USA* 101(34):12682–12687.
8. Best JL, et al. (2004) Identification of small-molecule antagonists that inhibit an activator: Coactivator interaction. *Proc Natl Acad Sci USA* 101(51):17622–17627.
9. Vidler LR, Brown N, Knapp S, Hoelder S (2012) Druggability analysis and structural classification of bromodomain acetyl-lysine binding sites. *J Med Chem* 55(17):7346–7359.
10. Filippakopoulos P, et al. (2010) Selective inhibition of BET bromodomains. *Nature* 468(7327):1067–1073.
11. Nicodeme E, et al. (2010) Suppression of inflammation by a synthetic histone mimic. *Nature* 468(7327):1119–1123.
12. Picaud S, et al. (2013) PFI-1, a highly selective protein interaction inhibitor, targeting BET Bromodomains. *Cancer Res* 73(11):3336–3346.
13. Dawson MA, et al. (2011) Inhibition of BET recruitment to chromatin as an effective treatment for MLL-fusion leukaemia. *Nature* 478(7370):529–533.
14. Hewings DS, et al. (2011) 3,5-dimethylisoxazoles act as acetyl-lysine-mimetic bromodomain ligands. *J Med Chem* 54(19):6761–6770.
15. Hay DA, et al. (2014) Discovery and optimization of small-molecule ligands for the CBP/p300 bromodomains. *J Am Chem Soc* 136(26):9308–9319.
16. Rooney TP, et al. (2014) A series of potent CREBBP bromodomain ligands reveals an induced-fit pocket stabilized by a cation-π interaction. *Angew Chem Int Ed Engl* 53(24):6126–6130.
17. Mele DA, et al. (2013) BET bromodomain inhibition suppresses TH17-mediated pathology. *J Exp Med* 210(11):2181–2190.
18. Korn T, Bettelli E, Oukka M, Kuchroo VK (2009) IL-17 and Th17 Cells. *Annu Rev Immunol* 27:485–517.
19. Shen H, Goodall JC, Hill Gaston JS (2009) Frequency and phenotype of peripheral blood Th17 cells in ankylosing spondylitis and rheumatoid arthritis. *Arthritis Rheum* 60(6):1647–1656.
20. Bowness P, et al. (2011) Th17 cells expressing KIR3DL2+ and responsive to HLA-B27 homodimers are increased in ankylosing spondylitis. *J Immunol* 186(4):2672–2680.
21. Sieper J (2013) Treatment challenges in axial spondylarthritis and future directions. *Curr Rheumatol Rep* 15(9):356.
22. Baeten D, et al. (2013) Anti-interleukin-17A monoclonal antibody secukinumab in treatment of ankylosing spondylitis: A randomised, double-blind, placebo-controlled trial. *Lancet* 382(9906):1705–1713.
23. Wei G, et al. (2009) Global mapping of H3K4me3 and H3K27me3 reveals specificity and plasticity in lineage fate determination of differentiating CD4+ T cells. *Immunity* 30(1):155–167.
24. Wang X, et al. (2012) Transcription of Il17 and Il17f is controlled by conserved noncoding sequence 2. *Immunity* 36(1):23–31.
25. Philpott M, et al. (2014) Assessing cellular efficacy of bromodomain inhibitors using fluorescence recovery after photobleaching. *Epigenetics Chromatin* 7:14.
26. Ciceri P, et al. (2014) Dual kinase-bromodomain inhibitors for rationally designed polypharmacology. *Nat Chem Biol* 10(4):305–312.
27. Berg EL, et al. (2010) Chemical target and pathway toxicity mechanisms defined in primary human cell systems. *J Pharmacol Toxicol Methods* 61(1):3–15.
28. Roderick JE, et al. (2014) c-Myc inhibition prevents leukemia initiation in mice and impairs the growth of relapsed and induction failure pediatric T-ALL cells. *Blood* 123(7):1040–1050.
29. Matzuk MM, et al. (2012) Small-molecule inhibition of BRDT for male contraception. *Cell* 150(4):673–684.
30. Reveille JD, Weisman MH (2013) The epidemiology of back pain, axial spondyloarthritis and HLA-B27 in the United States. *Am J Med Sci* 345(6):431–436.
31. Dean LE, et al. (2014) Global prevalence of ankylosing spondylitis. *Rheumatology (Oxford)* 53(4):650–657.
32. Cortes A, et al.; International Genetics of Ankylosing Spondylitis Consortium (IGAS); Australo-Anglo-American Spondyloarthritis Consortium (TASC); Groupe Française d'Etude Génétique des Spondylarthrites (GFEGS); Nord-Trøndelag Health Study (HUNT); Spondyloarthritis Research Consortium of Canada (SPARCC); Wellcome Trust Case Control Consortium 2 (WTCCC2) (2013) Identification of multiple risk variants for ankylosing spondylitis through high-density genotyping of immune-related loci. *Nat Genet* 45(7):730–738.
33. Evans DM, et al.; Spondyloarthritis Research Consortium of Canada (SPARCC); Australo-Anglo-American Spondyloarthritis Consortium (TASC); Wellcome Trust Case Control Consortium 2 (WTCCC2) (2011) Interaction between ERAP1 and HLA-B27 in ankylosing spondylitis implicates peptide handling in the mechanism for HLA-B27 in disease susceptibility. *Nat Genet* 43(8):761–767.
34. McInnes IB, et al.; PSUMMIT 1 Study Group (2013) Efficacy and safety of ustekinumab in patients with active psoriatic arthritis: 1 year results of the phase 3, multicentre, double-blind, placebo-controlled PSUMMIT 1 trial. *Lancet* 382(9894):780–789.
35. Burmester GR, et al.; EARTH Study Group (2013) Efficacy and safety of mavrilimumab in subjects with rheumatoid arthritis. *Ann Rheum Dis* 72(9):1445–1452.
36. Jandus C, et al. (2008) Increased numbers of circulating polyfunctional Th17 memory cells in patients with seronegative spondylarthritides. *Arthritis Rheum* 58(8):2307–2317.
37. Ciofani M, et al. (2012) A validated regulatory network for Th17 cell specification. *Cell* 151(2):289–303.
38. Gaffen SL, Jain R, Garg AV, Cua DJ (2014) The IL-23-IL-17 immune axis: From mechanisms to therapeutic testing. *Nat Rev Immunol* 14(9):585–600.
39. Byun JS, et al. (2009) Dynamic bookmarking of primary response genes by p300 and RNA polymerase II complexes. *Proc Natl Acad Sci USA* 106(46):19286–19291.
40. Annunziato F, et al. (2007) Phenotypic and functional features of human Th17 cells. *J Exp Med* 204(8):1849–1861.
41. Pène J, et al. (2008) Chronically inflamed human tissues are infiltrated by highly differentiated Th17 lymphocytes. *J Immunol* 180(11):7423–7430.
42. Matusevicius D, et al. (1999) Interleukin-17 mRNA expression in blood and CSF mononuclear cells is augmented in multiple sclerosis. *Mult Scler* 5(2):101–104.
43. Fedorov O, Niesen FH, Knapp S (2012) Kinase inhibitor selectivity profiling using differential scanning fluorimetry. *Methods Mol Biol* 795:109–118.
44. Kabsch W (2010) Xds. *Acta Crystallogr D Biol Crystallogr* 66(Pt 2):125–132.
45. Evans PR (2011) An introduction to data reduction: Space-group determination, scaling and intensity statistics. *Acta Crystallogr D Biol Crystallogr* 67(Pt 4):282–292.
46. Langer G, Cohen SX, Lamzin VS, Perrakis A (2008) Automated macromolecular model building for X-ray crystallography using ARP/wARP version 7. *Nat Protoc* 3(7):1171–1179.
47. Emsley P, Cowtan K (2004) Coot: Model-building tools for molecular graphics. *Acta Crystallogr D Biol Crystallogr* 60(Pt 12 Pt 1):2126–2132.
48. Murshudov GN, Vagin AA, Dodson EJ (1997) Refinement of macromolecular structures by the maximum-likelihood method. *Acta Crystallogr D Biol Crystallogr* 53(Pt 3):240–255.
49. Schüttelkopf AW, van Aalten DM (2004) PRODRG: A tool for high-throughput crystallography of protein-ligand complexes. *Acta Crystallogr D Biol Crystallogr* 60(Pt 8):1355–1363.
50. Chen VB, et al. (2010) MolProbity: All-atom structure validation for macromolecular crystallography. *Acta Crystallogr D Biol Crystallogr* 66(Pt 1):12–21.
51. Martinez FO (2012) Analysis of gene expression and gene silencing in human macrophages. *Curr Protoc Immunol*, Suppl 96, Unit 14.28, pp 14.28.1–14.28.23.